CrystEngComm c3ce41524d

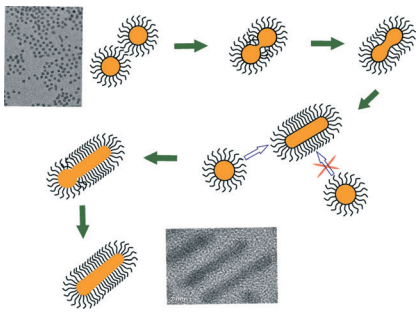

Surface ligand mediated growth of CuPt nanorods

Fengjiao Yu, Xiaoxiang Xu, Christopher J. Baddeley, Ronan M. Bellabarba, Pascal Lignier, Robert P. Tooze, Federica Fina, John S. T. Irvine and Wuzong Zhou*

A ligand mediated growth mechanism is proposed for non-orientated 1D assembly of CuPt nanoparticles.

Please check this proof carefully. **Our staff will not read it in detail after you have returned it.**

Translation errors between word-processor files and typesetting systems can occur so the whole proof needs to be read. Please pay particular attention to: tabulated material; equations; numerical data; figures and graphics; and references. If you have not already indicated the corresponding author(s) please mark their name(s) with an asterisk. Please e-mail a list of corrections or the PDF with electronic notes attached – do not change the text within the PDF file or send a revised manuscript. Corrections at this stage should be minor and not involve extensive changes. All corrections must be sent at the same time.

Please bear in mind that minor layout improvements, e.g. in line breaking, table widths and graphic placement, are routinely applied to the final version.

Please note that, in the typefaces we use, an italic vee looks like this: v, and a Greek nu looks like this: ν.

We will publish articles on the web as soon as possible after receiving your corrections; **no late corrections will be made.**

Please return your **final** corrections, where possible within **48 hours** of receipt, by e-mail to: crystengcomm@rsc.org

Queries for the attention of the authors

Journal: CrystEngComm

Paper: c3ce41524d

Title: Surface ligand mediated growth of CuPt nanorods

Editor's queries are marked on your proof like this Q1, Q2, etc. and for your convenience line numbers are indicated like this 5, 10, 15, ...

Please ensure that all queries are answered when returning your proof corrections so that publication of your article is not delayed.

Query Reference	Query	Remarks
Q1	For your information: You can cite this article before you receive notification of the page numbers by using the following format: (authors), CrystEngComm, (year), DOI: 10.1039/c3ce41524d.	
Q2	Please carefully check the spelling of all author names. This is important for the correct indexing and future citation of your article. No late corrections can be made.	

CrystEngComm

PAPER

Surface ligand mediated growth of CuPt nanorods†

Cite this: DOI: 10.1039/c3ce41524d

Fengjiao Yu,[a] Xiaoxiang Xu,[a] Christopher J. Baddeley,[a] Ronan M. Bellabarba,[b] Pascal Lignier,[b] Robert P. Tooze,[b] Federica Fina,[a] John S. T. Irvine[a] and Wuzong Zhou*[a]

Received 31st July 2013,
Accepted 4th December 2013

DOI: 10.1039/c3ce41524d

www.rsc.org/crystengcomm

CuPt alloy nanorods have been synthesized *via* one dimensional assembly of randomly orientated nanocrystallites in the presence of hexadecanoic acid and hexadecylamine as surface ligands. When hexadecanoic acid was added into the synthetic system first followed by a second step of adding hexadecylamine, strands of ultrathin CuPt nanowires were produced. The roles of the amine and organic acid are discussed. A novel ligand mediated mechanism is proposed, in which the formation of a stable monolayer structure of the ligands is the driving force to guide the 1D growth of the alloy nanorods without the influence of the crystal orientation. Photocatalytic hydrogen production from water has been performed using CuPt nanorods as a cocatalyst, which has a higher production rate (234.08 μmol h^{-1} g^{-1}) than that of Pt nanorods under the same conditions (~66.35 μmol h^{-1} g^{-1}). Our results suggest that polycrystalline CuPt nanorods with a large amount of defects are probably promising cocatalyst for photocatalysis.

Introduction

One dimensional nanomaterials possessing nanowire and nanorod morphologies exhibit novel optical and electrical properties,[1] which could be exploited in sensing,[2] memory and logic circuits[3] and so on. On the other hand, Pt based nanoparticles are important and effective catalysts that have been widely utilized in applications such as oxygen reduction reaction (ORR) in polymer electrolyte membrane fuel cells (PEMFCs),[4] methanol oxidation,[5] heterogeneous NO_x reduction[6] and a cocatalyst for hydrogen production in photocatalytic water splitting.[7,8] Additionally, one dimensional (1D) nanowires composed of noble metals, especially Pt and Pd, have shown enhanced catalytic performance dependent on structure and composition.[9–12]

A variety of methods have been demonstrated to achieve anisotropic nanomaterials. Template directed synthesis is one of the most widely reported approaches. The morphology of nanomaterials is controlled by templates, which could be stepped solid substrates,[13] porous materials with channels[14] or micelles self-assembled by surfactant molecules. As an example of the latter, Murphy and co-workers[15] synthesized gold nanorods, directed by cetyltrimethylammonium bromide (CTAB), that organized into rod-like micelles. The vapor–liquid–solid (VLS) method is another versatile way, generating single crystalline nanowires with the assistance of a catalyst droplet. In the VLS method, gaseous reactants first dissolve into liquid droplets, followed by nucleation and growth at the solid–liquid interface. The diameter of the nanowires produced by this method is obviously governed by the size of the catalytic particles.[14,16] Similarly, in the growth of C_{60} nanowires *via* evaporation of the solvent film, the diameter of the nanowires is limited by the thickness of the solvent film.[17,18] Cu-based bimetallic nanorods have been prepared with a noble metal as the seed and Cu atoms being reduced and nucleating on one side of the seed.[19] The formation process of Pt_3Fe nanorods *via* attachment of nanoparticle building units was observed by real time imaging.[20]

Anisotropic materials fabricated by self-assembly of nanoparticles *via* oriented attachment (OA) are also in abundance ever since Penn and Banfield[21,22] proposed the mechanism. In the OA growth, adjacent primary particles assemble *via* sharing the same crystallographic orientation. The critical issue about assembly of nanoparticles to form a 1D structure is why the material grows in one dimension. For example, metal nanowires often grow along the [111] zone axis of their face-centred cubic structures. However, there are three other <111> directions with an interplane angle of 70.52° with the [111] growing direction. It was not well elucidated why the nanowires grow along only one selected direction. Two principal mechanisms have been proposed recently. One is that

[a] *EaStCHEM, School of Chemistry, University of St Andrews, St Andrews, KY16 9ST, UK. E-mail: wzhou@st-andrews.ac.uk; Fax: +44 (0)1334 463808; Tel: +44 (0)1334 467276*
[b] *Sasol Technology (UK) Ltd, Purdie Building, St Andrews, KY16 9ST, UK*

† Electronic supplementary information (ESI) available: Chemical compositions of synthetic systems, EDX, TEM/HRTEM images, TGA, and FTIR results. See DOI: 10.1039/c3ce41524d

capping agents can preferentially bind to some specific facets, so that fusion occurs between planes with fewer capping agents on them.[23,24] The other is that dipole interaction drives the formation of a 1D structure, particularly for semiconductors.[25–27] These mechanisms cannot explain the 1D growth without branches of metal nanowires with a highly symmetric crystal structure. Furthermore, there are few examples of ligand-dominated formation of nanorods or nanowires with non-uniform crystallographic orientations.

Controllable and facile synthesis of bimetallic Pt-based nanomaterials may be an important route to maintain both desirable catalytic performance and low cost of the catalyst.[28] In particular, 1D alloy nanostructures are even more interesting, but controllable synthesis of uniform bimetallic nanorods and nanowires remains challenging.

Herein, we investigate the formation and growth process of CuPt nanorods, revealing a ligand mediated mechanism, in which 1D growth of the alloy nanorods is achieved by assembly of spherical nanocrystallites with very little influence of the crystal orientation. We suppose that the surface coating layer of mixed ligand molecules plays a critically important role. In addition, the use of these CuPt nanorods as a cocatalyst for photocatalytic hydrogen production from water was also investigated. Photocatalytic water splitting has been attracting a lot of attention because of its potential application for the production of a green fuel hydrogen[29] by using only water and sunlight. Until today, many catalysts have been discovered that are able to produce hydrogen from water by just exploiting light irradiation, but most of them are only active under UV-light (for example TiO_2 (ref. 29 and 30)). Unfortunately, just 4% of the solar spectrum corresponds to UV. Therefore, there is the need to find catalysts able to produce hydrogen by using visible light. The prerequisites for a catalyst to perform water splitting and hydrogen production are to have a band gap wider than the energy barrier for water splitting (1.23 eV) and a conduction band more negative than the reduction potential of water (0 V/NHE). Graphitic carbon nitride (g-C_3N_4) fulfils all these requirements. It is a semiconductor with a graphitic-like structure and its nitrogen and carbon p_z orbitals give it a band gap of 2.7 eV,[31] which makes it able to absorb visible light and subsequently reduce water. For these reasons, it was chosen as the catalyst in this study; however, g-C_3N_4 by itself does not show particularly good performances. It needs the aid of a co-catalyst and platinum has been demonstrated to be the best.[32] In this study, the use of a bimetallic system as a cocatalyst is investigated. The results obtained were promising and the CuPt nanorods showed better performances than Pt nanorods. Possible reasons for the higher activity in comparison with pure Pt nanorods synthesized with the same method are discussed.

Results and discussion

CuPt nanorods with dimensions of 15.7 ± 2.5 nm in length and 2.1 ± 0.2 nm in width were obtained after 0.5 h reaction in a synthetic system containing platinum acetylacetonate [$Pt(acac)_2$], copper acetylacetonate [$Cu(acac)_2$], 1,2-decanediol, hexadecanoic acid, hexadecylamine and diphenyl ether (see ESI†). A representative transmission electron microscopic (TEM) image is displayed in Fig. 1(a). A fraction of CuPt nanospheres with a diameter of 2.8 ± 0.2 nm (Fig. 1d) are contained in the as-synthesized product and can be separated in a further purification step by centrifugation. Upon increasing the reaction time up to 3 h, a large amount of nanospheres were still observed from the as-prepared sample. The high resolution TEM (HRTEM) image in Fig. 1(e) shows three CuPt nanorods with lattice fringes. A *d*-spacing of 0.218 nm, marked by the arrows, was measured from the fringes, corresponding to the (111) plane of CuPt alloy. The composition was confirmed by the energy-dispersive X-ray spectroscopy (EDX) result, which indicates a Cu : Pt atomic ratio of 46 : 54, matching a nearly 1 : 1 CuPt alloy. It is obvious that the crystallographic orientations of the nanorods are not uniform.

Due to their uniform size, both nanospheres and nanorods are well aligned on the carbon film *via* self-organization during the evaporation of solvent from the colloidal solution (Fig. 1a). It is noticed that particles are separated with an apparently uniform spacing of ~2.3 nm. This inter-particle spacing is presumably maintained by hexadecanoic acid and hexadecylamine on the surface, and the existence of these two capping agents was confirmed by the infrared study below. The length of the alkyl chain of the capping agents is estimated to be ~1.9 nm long indicating that the hydrocarbon chains of capping agents are interdigitated.[33,34] This inter-particle distance also indicates that a monolayer of ligands covers the surfaces of these nanorods.

Most nanospheres are polycrystalline and, when no nanorods are present, can self-assemble into a close-packed

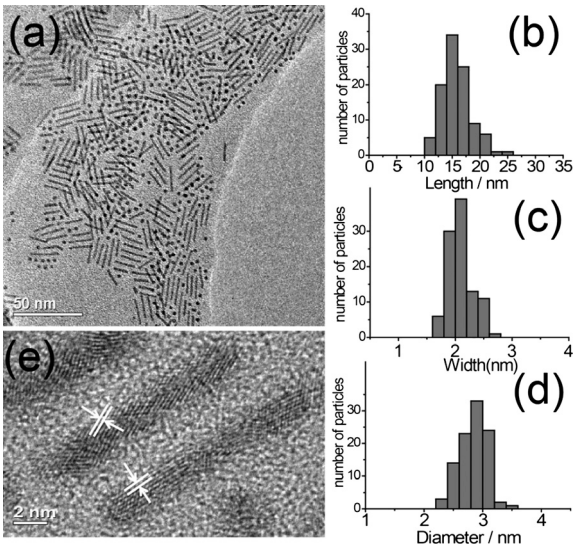

Fig. 1 (a) TEM image of as-prepared CuPt specimen after reaction for 0.5 h. Histograms are presented, (b) length of nanorods, (c) width of nanorods and (d) diameter of nanospheres. (e) HRTEM image of three nanorods. The fringes with a *d*-spacing of 0.218 nm corresponding to the (111) planes of CuPt are marked by the arrows.

monolayer or double-layered superstructure as shown in Fig. S1 (ESI†). A single crystal can possess faceted polyhedral morphology.[35] However, HRTEM image in Fig. S1a† reveals that the nanoparticles are small and have a polycrystalline nature. In this case, most particles have no obvious facets and are almost spherical.

Formation of CuPt nanorods

In order to investigate the growth mechanism of the CuPt nanorods, intermediates were collected in the heating process at 10, 15 and 25 min after the mixture was completely dissolved at 120 °C. At 10 min, it appeared that only very small CuPt nanoparticles were formed (Fig. 2a). These nanoparticles continued to grow to an average diameter of 2.1 ± 0.2 nm as observed in the 15 min sample (Fig. 2b). In contrast to the nanospheres in the 0.5 h product (Fig. 1d) with an average diameter of 2.8 nm, the nanoparticles in the 15 min sample have smaller size, poor crystallinity and less regular shape. They randomly sit on the carbon film, indicating that there is no dense surface coating layer of ligands on these low crystallinity nanoparticles, and they more likely consist of partially reduced metal clusters.

After 25 min, a monolayer of CuPt nanospheres assembled in a close-packed manner on the carbon film of the TEM specimen grid. Nanorods with different lengths appeared as well (Fig. 2c). Many of them are obviously shorter but wider than the ones in the final product. A scatter diagram plotting the length against the width of the nanorods in Fig. S2 (ESI†) indicates that width decreases with increasing length. It excludes the possibility of seeded growth, in which the width should remain at least unchanged, if not increased.[19] Even in the product when the reaction time was extended to 3 h, we observed polycrystalline rods with obvious boundaries (arrows A) and single crystalline domain (arrow B), as seen in the HRTEM image (Fig. 2d), which would not appear if the growth is a seeded mechanism.

Fig. 3(a) shows some short nanorods. One of them marked by a rectangle consists of two nanospheres just joined together to form a dumbbell shaped nanorod. Atoms sited on the surface of the spheres would move to the joint of the dumbbell particles to fill the concave space. Consequently, the diameter of the newly formed rod is smaller than that of the original spheres (Fig. 3).

The above observations suggest that nanospheres act as building units to form rods. Further, the Ostwald ripening process produces single crystalline domains, by fusion of the spherical crystallites in the rods. Short rods grow faster than the longer ones due to the diffusion-controlled growth, and as a result, size distribution can be narrowed down, a situation similar to the "focusing" effect.[36]

Crystallographic orientation of nanorods

The most reported one-dimensional growth of materials is usually along a specific crystallographic orientation to eliminate high energy facets, such as growth along the [001] zone axis of TiO_2 nanorods and [111] of Au nanowires, *etc.*[23,24] However, it appears that the nanorods in the present work did not grow along a uniform crystal zone axis. Fig. 3(b) shows some nanorods with growth direction perpendicular to [111] as indicated by an arrow, which could most likely be the [110] or [211] direction. Some more examples are shown in Fig. 1(e) and in Fig. S3 (ESI†).

The XRD pattern in Fig. 4 shows broadening peaks, from which the calculated crystal size is about 2 nm in all zone axes according to the Scherrer equation. It excludes the possibility of unidirectional growth, in which case a sharpened peak could be expected in the growth direction.[37] Moreover, HRTEM images reveal that rods are built up by several primary spheres with different orientations, which implies that

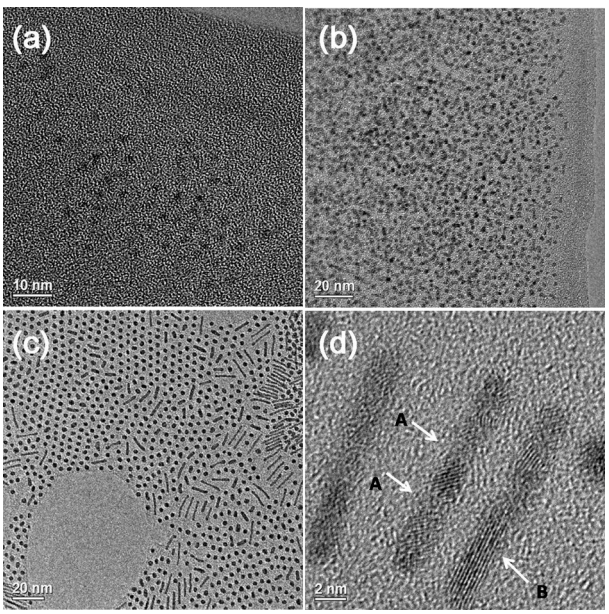

Fig. 2 TEM images of nanorod intermediates observed after heating for (a) 10 min, (b) 15 min, (c) 25 min. (d) Nanorods with boundaries (indicated by A arrows) between nanocrystallites and single crystalline domain (indicated by B arrow) from the final product with reaction time of 3 h.

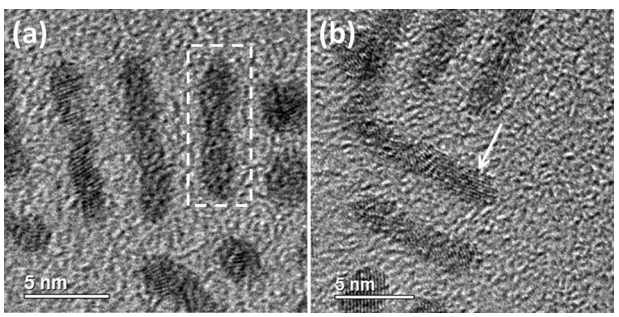

Fig. 3 HRTEM images of some nanorods from 1 : 1.5 sample, showing the early stage formation of the nanorods. The particle marked in (a) shows a dumbbell shape formed by a combination of two nanospheres. The arrow in (b) indicates lattice fringes of the (111) planes of CuPt alloy.

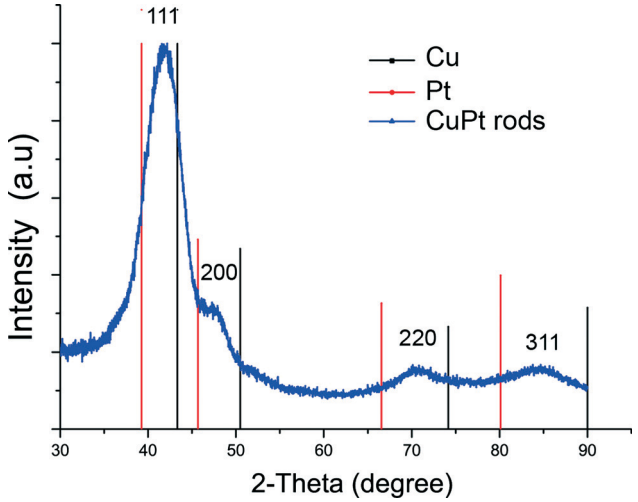

Fig. 4 XRD pattern of CuPt nanorods. Red and black lines indicate peak positions of pure Pt and Cu respectively.

crystallographic orientation is not the dominant factor in the growth of nanorods. The one dimensional assembly of the nanocrystallites must result from other factors.

Effect of alkyl chain of ligands

Replacing hexadecylamine/hexadecanoic acid by similar amine and acid with different alkyl chain lengths can significantly change the lengths of produced nanorods (Fig. 5). The use of octylamine and octanoic acid (C8) leads to formation of nanorods of 9.5 ± 1.8 nm in length. Using dodecylamine and dodecanoic acid (C12) increases the length of nanorods to 11.4 ± 1.6 nm. Replacement of amine and acid by octadecylamine and stearic acid (C18), respectively, yields nanorods of 15.2 ± 3.0 nm in length. The relationship between length of the nanorods and alkyl chain of ligands is summarized in Fig. 5(d). The average inter-particle spacings of nanorods prepared with C8, C12 and C18 are 1.9 nm, 2.0 nm and 2.3 nm, respectively. The length of nanorods can be simply tuned by changing the capping agents. Since the ligands used in these syntheses only differ in alkyl chain, their chemical properties should remain similar. This indicates that the growth of nanorods is controlled by supramolecular organization of the ligands.[38] Ligand–ligand interaction is enhanced with increasing length of alkyl chain. Longer rods are stabilized by the short distance interactions between alkyl chains of the surface ligands. However, very long alkyl chains may have difficulties in ordering. In the present work, changing the alkyl chain lengths of acid and amine from C16 to C18 did not lead to longer nanorods.

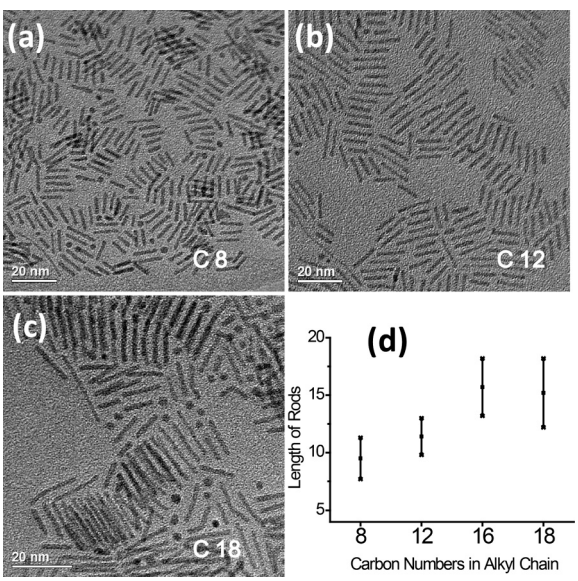

Fig. 5 TEM images of CuPt nanorods synthesized with (a) octylamine and octanoic acid (C8), (b) dodecylamine and dodecanoic acid (C12), and (c) octadecylamine and stearic acid (C18). (d) Variation of length of nanorods dependent on the length of ligands.

Effect of concentration of ligands

We regard the first preparation conditions with the ratio of metal : amine : acid = 1 : 9 : 9 as the standard conditions (amine : acid = 1 : 1 sample in ESI,† Table S1). Raising the amine/acid ratio to 1.5 : 1 simply by increasing the amount of amine, nanorods with average length of 24.3 ± 5.3 nm were synthesized (ESI,† Fig. S4). Nanorods of 28.9 ± 9.4 nm could be yielded by further increasing the amount of amine to an amine : acid ratio of 2 : 1 (Fig. 6b). Increasing the amount of amine will lead to longer rods, a trend also reported by others.[28,39] The roles of the capping agents, however, have not been elucidated.

With further experiments, we found that, in the sample of amine : acid = 1 : 1.5, increasing the amount of acid resulted in shorter rods with an average length of 11.7 ± 2.0 nm (Fig. 6a). With constant ratio of amine : acid = 1 : 1, increasing the amount of both capping agents to 1.5 (amine : acid = 1.5 : 1.5) leads to rods with a length of 24.0 ± 5.2 nm (Fig. 6d), similar to the length of rods produced with amine : acid = 1.5 : 1. Decreasing both capping agents to 0.5 (amine : acid = 0.5 : 0.5) resulted in the specimen containing mainly smaller spherical particles (~2 nm) (Fig. 6c). Uniform nanospheres and a small amount of very short rods are formed in the presence of acid alone (Fig. 6e). When amine is used as the sole capping agent, the metal precursors were decomposed/reduced at a lower temperature (~130 °C) and nanoparticles with wide size distribution are formed (Fig. 6f).

Our observation of the early stage growth of nanospheres indicated that the metal precursor molecules and organic ligands may aggregate at the first step, followed by decomposition and reduction of the precursor molecules. Further growth of the metal nanospheres may rely on deposition of metal precursor molecules, in which metals may not yet fully be reduced to zero-valent atoms. This phenomenon was supported by theoretical studies,[40,41] demonstrating that addition of ions to growing clusters occurs before their reduction. HRTEM images also revealed a low crystallinity in the early stage particle (ESI,† Fig. S1). Therefore, the

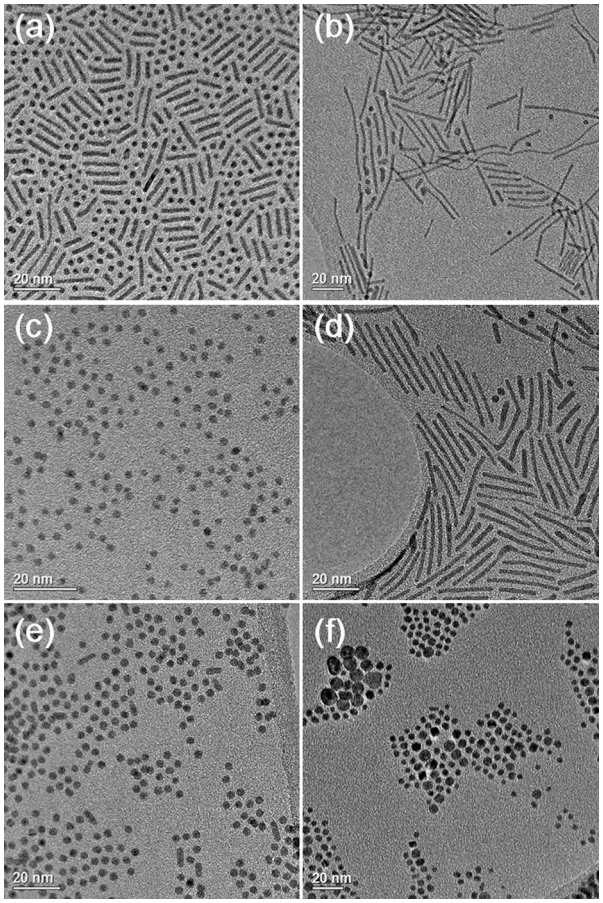

Fig. 6 TEM images of CuPt nanoparticles prepared with different amounts of amine and acid. Amine : acid ratios (a) 1 : 1.5, (b) 2 : 1, (c) 0.5 : 0.5, (d) 1.5 : 1.5, (e) acid alone, and (f) amine alone.

nanospheres may contain partially reduced Pt and Cu cations. This state prefers surface absorption of organic acidic molecules which have a negatively charged carboxylic group. It could be one reason explaining why acid acts as a stronger ligand than amine. Consequently, uniform sized nanospheres can form in the acid-only system (Fig. 6e), but not in the amine-only system (Fig. 6f).

As the alloy nanospheres are gradually reduced, surface adsorption of mixed amine and acid would be preferred. It has been calculated that adsorption of the amine functional group is more favored than the carboxylic acid group on zero-valent PtAg surface.[42] We can expect a similar situation in CuPt rods. Increasing amine concentration facilitates amine adsorption, probably with partial replacement of surface acid, leading to elongation of nanorods due to the increase of surface ligand density. Experimental evidence from IR characterization is displayed in later section. On the other hand, increasing acid concentration in solution has little effect on the increasing density of surface ligands. As a result, nanorods retain their length in spite of extra acid.

As capping agents help to decrease the monomer oversaturation,[43] in the case of half the amount of amine and acid (0.5 : 0.5 in Fig. 6c), nucleation is less suppressed. Consequently, a larger number of smaller spheres are yielded. The surfaces of these nanospheres are loosely bound, thus interactions between ligands are drastically weakened. As a consequence, these ligands on the surface are insufficient to drive the formation of nanorods. Adding acid alone did not produce nanorods. This can be caused by the reduced surface density of ligands.

In summary, the initial concentration of amine and acid determines the ligand density on the surface of the spheres, which has a crucial role in subsequent formation of the nanorods.

Two-step synthesis of CuPt nanowires

To verify the mechanism, a two-step synthesis was conducted. Acid was used as capping agent in the first step, producing mainly nanospheres as previously discussed (Fig. 6e and 7a). Then, amine was added into the mixture at room temperature and heated up to repeat the procedure. Surprisingly, strands of ultrathin CuPt with a diameter of 1.5 nm nanowires were formed incorporating some nanospheres. The TEM image in Fig. 7(b) shows such a particle made from CuPt nanowires. The total length of these strand particles can be as long as dozens of micrometers. Fig. 7(c) shows a TEM image, demonstrating how multiple ultrathin wires stagger and elongate to form large pieces. Crystal fringes are observed from the HRTEM image (Fig. 7d), showing the relatively high crystallinity of these nanowires. EDX analysis shows a Cu : Pt ratio of ~42 : 58, as shown in Fig. S5 (ESI†). Amine did not participate in the nucleation process in this two-step synthesis. The starting reactants were as-formed

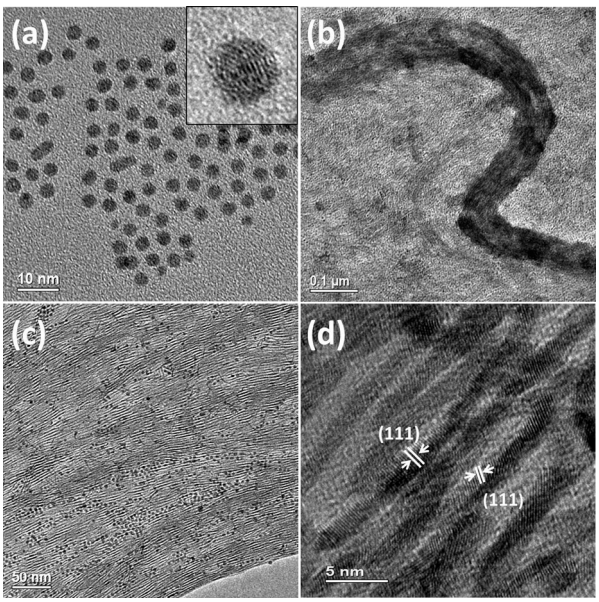

Fig. 7 TEM image of (a) CuPt nanoparticles produced with acid alone in the first step; inset is HRTEM image of a sphere with lattice fringes. (b) A strand-like particle of CuPt nanowires synthesized with the two-step method. (c) TEM and (d) HRTEM images of ultrathin nanowires inside the strand-like particle.

nanospheres as shown in Fig. 7(a); they had been reduced to nanocrystals and the lattice fringes can be observed (inset of Fig. 7a). Therefore, the elongation could only be induced by addition of amine without adding more metal precursors.

This two-step method can also be applied to nanospheres prepared with amine : acid = 0.5 : 0.5. Using these nanospheres as starting materials and adding amine and acid in the second step, elongated nanorods were produced (ESI,† Fig. S6). The nucleation environment was exactly the same as that in one-pot synthesis. Addition of ligands at the second step caused the formation of rods from spheres.

Both phenomena provide evidence for the sphere-to-rod mechanism mentioned previously in the standard one-pot synthesis. It is an interesting yet unanswered question that why adding amine into the suspension of nanospheres coated with acid allows us to produce very long CuPt nanowires. It is noteworthy that acid on these nanospheres has already organized into an ordered array to optimize intermolecular separations. Amine would likely insert or displace carboxylate species on the surface of the nanospheres. One assumption might be that the fast growth into long nanowires takes place during the invasion of the amine molecules.

It is obvious from the above work that surface ligands are crucial in 1D growth of CuPt nanorods. Experimental results imply that there is a threshold ligand density on surface to be satisfied for nanospheres before they will start to join together. Once the threshold density is reached, formation of nanorods can begin, in which process uniform crystallographic orientations are not required.

Coverage of ligands on surface

We also performed thermogravimetric analysis (TGA) and Fourier Transform Infrared (FTIR) characterization to confirm a dense layer of surface ligands and their interaction with the alloy particles. For the organization of ligand shell, direct observation by TEM is difficult in our experimental condition, because the surface ligand molecules are small and contain only light elements, giving very low image contrast. However, Rupar *et al.*[44] have shown TEM observations of cylindrical micelles with crystalline core and monolayer coil shell formed by self-assembly of block copolymers containing heavy atoms. We can expect similar monolayer of amine and acid ligand shell on the CuPt nanorods.

The TGA result from a specimen of 1 : 1 amine and acid (ESI,† Fig. S7) indicates a weight loss of 24.9%. The molecular weights of hexadecylamine and hexadecanoic acid are 241.5 and 256.4, respectively, resulting in an average molecular weight of ligand, 249.0. An average atomic weight of CuPt alloy is 129.3. Therefore, the weight loss of 24.9% observed from TGA corresponds to a ratio of the numbers of ligand molecules and metal, 0.17 : 1. Assuming the sample contains 25% nanospheres with the diameter of 2.8 nm and 75% nanorods with the length of 15.7 nm and the diameter of 2.1 nm. It is also assumed that the density of metal atoms on the (100) face of the face-centred cubic unit cell is applied to all the surfaces. 40% metal atoms are on surface. Consequently, the ratio of the ligand and surface metal atoms is 0.43 : 1. In this case, the density of the ligand molecules is about one molecule per two surface metal atoms. It is noteworthy that the amine : acid = 2 : 1 sample shows a weight loss of 32.2%, which is significantly larger compared to 1 : 1 specimen (ESI,† Fig. S7). This confirms our previous assumption that the density of surface ligands will increase with increasing amount of amine.

Fig. 8 shows some IR spectra from different samples. The commonly observed bands at about 2950, 2915 and 2848 cm^{-1} are from the asymmetric stretch of CH_3, asymmetric stretch of CH_2 and symmetric stretch of CH_2, respectively. The bands at 1473 and 1461 cm^{-1} may be assigned to the CH_2 scissor modes of the methylene units. All these bands can be expected for both the acid and the amine.

For the acid–amine mixture sample without nanorods (Fig. 8a), the absence of a band at 1700–1750 cm^{-1} is indicative that there is no free carbonyl band associated with –COOH.[45] The well-defined peak at 1639 cm^{-1} only appears in (a), and may be assigned to the $\delta_{asym}(NH_3^+)$ mode. The band at 1508 cm^{-1} is in the range of the symmetric NH_3^+ deformation.[46] The band at 1402 cm^{-1} probably corresponds to the symmetric stretch of the carboxylate. Therefore, the spectrum is consistent with a mixture of alkylammonium ions and carboxylate species.

For nanoparticles synthesized with only acid as shown in Fig. 8(b), the band at 2048 cm^{-1} is associated with adsorbed CO on Pt-like sites, probably due to decomposition of the acid molecules. The very weak 1699 cm^{-1} band (ν (C═O)) is from the presence of a small amount of carbonyl species – probably derived from a small amount of free acid. The relatively broad bands centred at 1560 cm^{-1} and 1416 cm^{-1} are characteristic of the ν_{asym} and ν_{sym} (OCO) of the adsorbed carboxylate. Indeed, the spectrum resembles very closely that

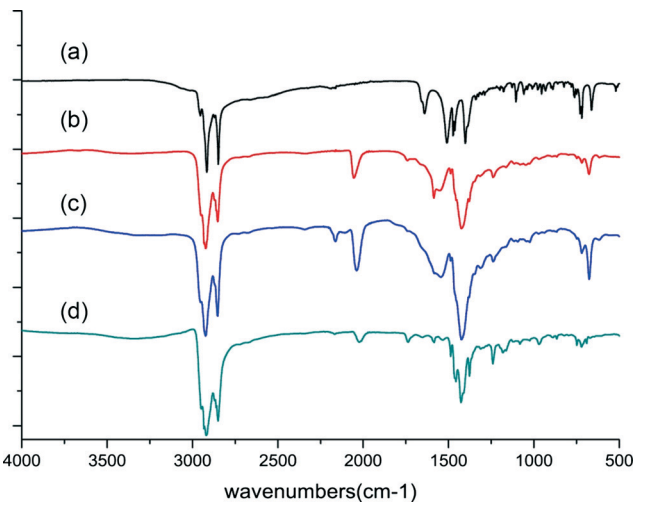

Fig. 8 IR spectra of (a) mixture of 1 : 1 acid and amine, (b) CuPt nanoparticles synthesized with acid alone, (c) CuPt nanorods from two-step synthesis with amine : acid = 1.5 : 1, and (d) CuPt nanorods synthesized with amine : acid = 1 : 1.

reported for hexadecanoate on aluminium.[47] This spectrum provides evidence that the acid bonds to the metal *via* carboxylate.

For the nanorods synthesized by the two-step method (Fig. 8c), in comparison with Fig. 8(b), there is a significant extra band at 2158 cm^{-1}, which is likely to be the C═N stretch of adsorbed nitrile formed from dehydrogenation of the amine.[48] We therefore can conclude that both acid and amine molecules are adsorbed on the metal surface. The IR spectrum of the sample with an amine : acid ratio of 1 : 1 (Fig. 8d) is similar to that in Fig. 8(c). In each case, the spectra are dominated by the presence of adsorbed carboxylate, but the 1550 cm^{-1} band is broadened at higher wavenumber which may suggest some contribution from amine or alkylammonium bands in the 1580–1630 cm^{-1} range implying some adsorption of amine or related species.

As the amine : acid ratio increases, *e.g.* in the samples of 1.5 : 1 and 2 : 1, the amine adsorption becomes more obvious and carboxylate adsorption becomes increasingly less apparent (ESI,† Fig. S8). The amine and acid appear to adsorb competitively such that the adsorption of amine is enhanced by increasing the concentration in the one-step synthesis to form more dense monolayers on the nanorod surface, resulting in longer nanorods.

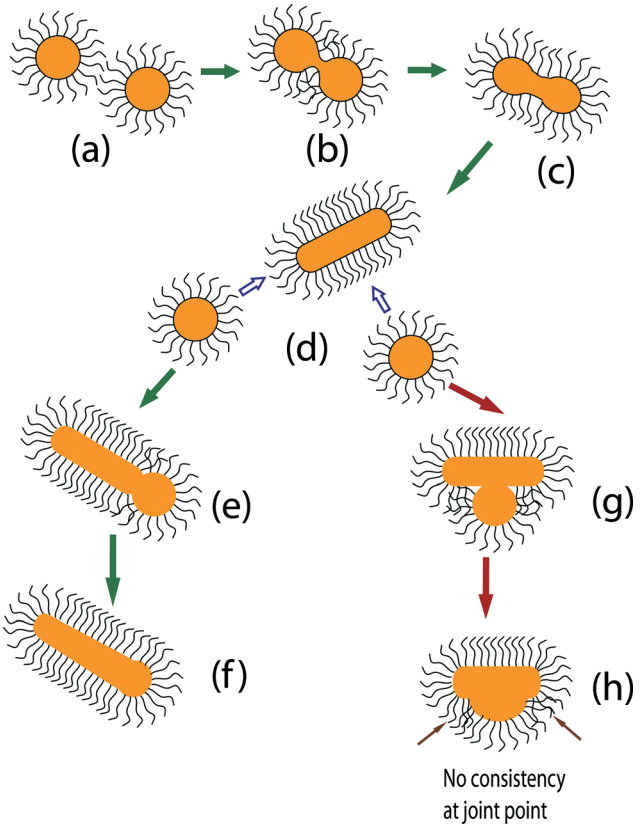

Scheme 1 Schematic drawing of one dimensional growth of nanorods controlled by the structure of surface ligands.

Discussion of formation mechanism of nanorods

Based on the observed growth patterns, we propose an attachment mechanism of nanocrystallites controlled by the organization of surface ligands. It has been previously proposed[23,25] that the anisotropic growth of nanorods could be caused by preferred coordination of ligands to specific facet or driven by dipole–dipole interaction. But, these are not the cases in the present work. Experimental evidence excludes the possibility of seeded growth or crystallographic orientation, and suggests that formation of a stable monolayer structure of organic capping agents is the driving force, as illustrated in Scheme 1.

The metallic surface of the nanospheres is bound with ligands, which are either the amine or the acid (or a mixture of both species), *via* the terminal functionality yielding densely packed surface coatings driven by significant van der Waals interactions between adjacent alkyl chains. The nanospheres diffuse in the solution randomly due to Brownian motion, solution convection and stirring, until two spheres collide and fuse to produce a dumbbell-like short nanorod (Scheme 1b). The fusion process of two spheres may involve the removal of surface ligands.[25] Atoms on the ends of the rod would migrate to the concave joint, which has lower chemical potential, leading to formation of circular cross sections with a uniform diameter (Scheme 1c, d). Under this circumstance, all the ligands are almost parallel to each other with stable distances on side surface, reducing the surface energy and stabilizing the side surface. A cylinder-like secondary particle (Scheme 1d) is formed with decreased total energy as a result of denser and ordered surface ligands, and elimination of the solid–liquid interface.[21] The nanorods are polycrystalline containing nanocrystallites with random orientations.

The attachment model can be analogously described by the Smoluchowski equation,[49] which has been proved to fit well for the attachment kinetics of organic ligand capped nanocrystals.[50,51] The model of the Smoluchowski equation involves monomer–monomer reaction and addition of monomer to multimer, and multimer–multimer reaction can be neglected.[50,52]

It is very unusual for primary spheres to attach in a linear manner, if there is no special force guiding such an interaction. We suspect that the total energy of surface molecular organization dominates the nanorod growth. If the third spherical particle joins the cylinder from a linear direction (Scheme 1e), a relatively uniform orientation of surface capping agents exists between primary and secondary particles (Scheme 1f), which guarantees the highest density of molecular binding to surface. In contrast, a primary sphere approaching the side surface of the cylinder to form a quasi-triangular shape (Scheme 1g) may undergo strong repulsive forces from adsorbed molecular species. In this case, the ligands at contact points between cylinder and sphere need complete rearrangement with the formation of a triangular plate as a prerequisite (Scheme 1h). Therefore, the route (d)–(e)–(f) in the scheme took place preferentially and the route (d)–(g)–(h) was hardly observed in the present work.

We also considered the effect of solvent, which may affect the interactions between ligands and alloy nanoparticles. Diphenyl ether (dipole moment is 1.05 D) and 1-octadecene (dipole moment is 0.47 D) were used as solvents for a comparison. We did not find any notable difference in the nanomaterials. We believe this is partially because the interaction between the ligand molecules and the CuPt particles are strong. In another experiment, we found that the solvent effect on the Pd-containing alloy nanoparticles is much more significant. This could be due to a relatively weak interaction between ligand molecules and alloy particles and, in that case, the interaction between the solvent and ligand molecules cannot be ignored.

All experimental results support this hypothesis, but theoretical calculation and simulation are needed to validate it. It is noteworthy that mathematical model has illustrated that the final aspect ratio is completely determined by the ratio of surface energy between side and cap surfaces, *i.e.* $S = S_{side}/S_{cap}$, in the case of Au nanorods.[53] This model does not put any restriction on the growth rates of different crystallographic directions, which is consistent with our mechanism.

Cocatalyst in photocatalytic hydrogen production from water

Cocatalysts play a crucial role in photocatalytic activity and product selectivity.[30] It is often observed that the performance of a semiconductor photocatalyst increases sharply as several orders of magnitude higher by loading appropriate cocatalysts. This is particularly evident in the case of graphitic carbon nitride.[7] Here, we use the as-prepared CuPt nanorods as a cocatalyst and load them on g-C_3N_4 for hydrogen production from water under visible light. Pure Pt nanorods were prepared with the same method but in the absence of Cu precursor (TEM images in ESI,† Fig. S8), and used for comparison. The results are displayed in Table 1.

It can be seen from Table 1 that the activity of g-C_3N_4 is considerably improved by loading either 1 wt% Pt or CuPt nanorods, indicating the effect of the cocatalyst. More interestingly, such an effect is more pronounced in the case of CuPt nanorods: the H_2 production rate is higher by a factor of 3.5 times than that of pure Pt nanorods, suggesting a positive effect of Cu into Pt structure. It is generally accepted that cocatalysts help to collect photo-generated charges on semiconductors and promote catalytic reactions.[30] Cu has a smaller work function than Pt (Cu: 4.53–5.10 eV, Pt: 5.12–5.93 eV),[54] therefore introducing Cu might be helpful to lower the Schottky barrier between the semiconductor g-C_3N_4 and metal CuPt, which is favourable for the transferring of photo-generated electrons from the g-C_3N_4 to CuPt nanorods. On the other hand, substitution of Pt with Cu breaks down the connection between adjacent Pt atoms in a manner similar to isolated Pt clusters. Such a "quantum size effect" might be another reason for the improved activity observed. Finally, the CuPt nanorods contain a large number of structural defects due to their polycrystalline nature, while the pure Pt nanorods have much higher crystallinity as shown in ESI,† Fig. S9. The positive effect of surface defects on the photocatalytic activity should not be ignored, although the mechanism is not well understood.

Table 1 Photocatalytic hydrogen production rate for samples with and without cocatalyst under visible light irradiation ($\lambda \geq 420$ nm)

Sample	H_2 production rate (μmol h^{-1} g^{-1} catalyst)
Pure g-C_3N_4	1.65
g-C_3N_4 + 1 wt% Pt nanorods	66.35
g-C_3N_4 + 1 wt% CuPt nanorods	234.08

Conclusions

One dimensional growth of CuPt nanorods was found to depend on the stable monolayer of surface ligands, by coalescence of nanospheres regardless of crystallographic orientations. The total energy of surface ligands plays a crucial part in assistance of the linear growth. Thus, the ligand–ligand interaction on surfaces determines the final length of the rod product. With this understanding, the length of the rods can be successfully tuned by varying the ratio, the alkyl chain length and the addition sequences of amine and acid ligands. This new mechanism allows insight into rational design of 1D nanomaterials. This work also implies that, when we try to understand formation of crystal morphology with the presence of surface ligands in the synthetic system, we should not ignore the contribution of the surface ligands to the total surface energy. CuPt nanorods show promising activity as a cocatalyst in photocatalytic hydrogen production from water. Our results suggest that metal alloys can be candidates for efficient cocatalysts and are worthy of further investigation for the development of active photocatalytic systems.

Experimental

Synthesis

CuPt nanorods were synthesized in the ambient atmosphere using a modified synthetic method originally reported by Liu *et al.*[28] 40 mg of platinum acetylacetonate [$Pt(acac)_2$], 26 mg of copper acetylacetonate [$Cu(acac)_2$], 70 mg of 1,2-decanediol, 460 mg of hexadecanoic acid and 450 mg of hexadecylamine were mixed with 5.0 mL of diphenyl ether in a round-bottom flask. The flask was heated to 120 °C until the solids were completely dissolved and the solution turned transparent blue. The solution was then heated to 225 °C and maintained for 30 min. A color change from blue to green, then to yellow and finally to black was observed during the heating process. The final solution was cooled down to room temperature and a black powder product was recovered by centrifugation. The as-synthesized specimens often contained nanospheres and nanorods of CuPt. The majority of nanospheres can be removed by adding cyclohexane and ethanol, followed by centrifugation. The supernatant contains

only nanospheres and the precipitate contains mainly nanorods. The precipitate can be well dispersed in cyclohexane. The solid specimens were washed by using ethanol to remove the remaining organic molecules.

We varied the initial amounts of hexadecanoic acid, hexadecylamine and 1,2-decanediol to systematically study their effects on synthesis. A two-step method was also applied to synthesize strands of ultrathin CuPt wires. The first step was the same as described above, except no hexadecylamine was added. The solution was cooled down to room temperature after 30 min reaction. In the second step, amine was added to the solution and the procedure was repeated. The detailed conditions for preparation of CuPt nanorods are summarized in Table S1 (ESI†). We also replaced the mixed ligands (hexadecanoic acid and hexadecylamine) by (octanoic acid, octylamine), (dodecylamine, dodecanoic acid) and (stearic acid, octadecylamine) with the same molar amount to study how the length of the surface ligands affect the growth of nanorods.

Pt nanorods for the catalysis test were prepared with the same method except for the absence of $Cu(acac)_2$ precursor. Graphitic carbon nitride (g-C_3N_4) was synthesized by melamine condensation.[55] Melamine (Aldrich 99%) was calcined in an alumina crucible covered with aluminium foil at 600 °C for 2 h. The resulting yellow powder was inspected by XRD and confirmed to be pure g-C_3N_4 phase.[7] Loading of cocatalysts (Pt or CuPt nanorods) onto the g-C_3N_4 was simply performed by dispersing the g-C_3N_4 and Pt or CuPt in cyclohexane solution. The dispersion solution was then dried at 100 °C and subsequent calcination at 180 °C for 2 hours.

Characterization

TEM and HRTEM images were obtained using a JOEL-2011 electron microscope operated at 200 kV. Samples were diluted in hexane and drop-cast onto a holey carbon-coated copper grid followed by solvent evaporation in air at room temperature. Metallic ratios in the samples were examined by EDX using an Oxford INCA system fitted in a Jeol JSM-6700F field emission scanning microscope operating. Powder XRD was performed using a PANalytical Empyrean diffractometer with Cu Kα radiation. Attenuated Total Reflection FTIR (ATR-FTIR) was performed using Thermo Fisher NICOLET 6700 FT-IR spectrometer. TGA was carried out using NETZSCH TG 209 instrument at a heating rate of 5 °C min^{-1} in air.

Photocatalytic hydrogen evolution

Measurement of photocatalytic hydrogen production was carried out using a home-made Teflon reactor.[56] In a typical experiment, 0.2 g catalyst was dispersed in 200 ml oxalic acid solution (0.025 M) and was sealed within the Teflon reactor. The reactor was then purged with pure Ar gas as a protective atmosphere. A 250 W iron doped metal halide UV-Vis lamp (Borosilicate Coated Glass HM07, UQG (optic) Ltd., Cambridge, UK) filtered with UV cut-off filter $\lambda \geq 420$ nm was used as light source. The photon flux of the lamp generated is calibrated using a quantum meter (Apogee MQ-200), which is 1305 ± 27 μmol m^{-2} s^{-1}. The gas composition within the reactor was monitored by using an on-line gas chromatograph (Aglient 3000 Micro Gas Chromatograph). The measurements were generally carried out for 20 hours and the average results were calculated and used in the manuscript.

Acknowledgements

FY thanks the University of St Andrews for SORS scholarship and Sasol Technology Ltd UK for financial support. WZ thanks EPSRC for financial support of the microscopy facility.

Notes and references

1 Y. Xia, P. Yang, Y. Sun, Y. Wu, B. Mayers, B. Gates, Y. Yin, F. Kim and H. Yan, *Adv. Mater.*, 2003, **15**, 353–389.
2 F. Patolsky and C. M. Lieber, *Mater. Today*, 2005, **8**, 20–28.
3 H. Yan, H. S. Choe, S. W. Nam, Y. J. Hu, S. Das, J. F. Klemic, J. C. Ellenbogen and C. M. Lieber, *Nature*, 2011, **470**, 240–244.
4 S. Koh and P. Strasser, *J. Am. Chem. Soc.*, 2007, **129**, 12624–12625.
5 D. Xu, Z. P. Liu, H. Z. Yang, Q. S. Liu, J. Zhang, J. Y. Fang, S. Z. Zou and K. Sun, *Angew. Chem., Int. Ed.*, 2009, **48**, 4217–4221.
6 S. Zhou, B. Varughese, B. Eichhorn, G. Jackson and K. McIlwrath, *Angew. Chem., Int. Ed.*, 2005, **44**, 4539–4543.
7 X. C. Wang, K. Maeda, A. Thomas, K. Takanabe, G. Xin, J. M. Carlsson, K. Domen and M. Antonietti, *Nat. Mater.*, 2009, **8**, 76–80.
8 X. X. Xu, C. Randorn, P. Efstathiou and J. T. S. Irvine, *Nat. Mater.*, 2012, **11**, 595–598.
9 Z. W. Chen, M. Waje, W. Z. Li and Y. S. Yan, *Angew. Chem., Int. Ed.*, 2007, **46**, 4060–4063.
10 S. J. Guo, S. Zhang, X. L. Sun and S. H. Sun, *J. Am. Chem. Soc.*, 2011, **133**, 15354–15357.
11 C. Koenigsmann, W. P. Zhou, R. R. Adzic, E. Sutter and S. S. Wong, *Nano Lett.*, 2010, **10**, 2806–2811.
12 H. W. Liang, X. A. Cao, F. Zhou, C. H. Cui, W. J. Zhang and S. H. Yu, *Adv. Mater.*, 2011, **23**, 1467–1471.
13 E. C. Walter, B. J. Murray, F. Favier, G. Kaltenpoth, M. Grunze and R. M. Penner, *J. Phys. Chem. B*, 2002, **106**, 11407–11411.
14 Z. X. Su, C. Dickinson, Y. Wan, Z. Wang, Y. Wang, J. Sha and W. Z. Zhou, *CrystEngComm*, 2010, **12**, 2793–2798.
15 C. J. Murphy, T. K. San, A. M. Gole, C. J. Orendorff, J. X. Gao, L. Gou, S. E. Hunyadi and T. Li, *J. Phys. Chem. B*, 2005, **109**, 13857–13870.
16 S. H. Xie, W. Z. Zhou and Y. Q. Zhu, *J. Phys. Chem. B*, 2004, **108**, 11561–11566.
17 J. F. Geng, W. Z. Zhou, P. Skelton, W. B. Yue, I. A. Kinloch, A. H. Windle and B. F. G. Johnson, *J. Am. Chem. Soc.*, 2008, **130**, 2527–2534.
18 Y. N. Zhou and W. Z. Zhou, *CrystEngComm*, 2012, **14**, 1449–1454.

19 S. Chen, S. V. Jenkins, J. Tao, Y. Zhu and J. Chen, *J. Phys. Chem. C*, 2013, **117**, 8924–8932.

20 H. G. Liao, L. K. Cui, S. Whitelam and H. M. Zheng, *Science*, 2012, **336**, 1011–1014.

21 R. L. Penn and J. F. Banfield, *Science*, 1998, **281**, 969–971.

22 J. F. Banfield, S. A. Welch, H. Z. Zhang, T. T. Ebert and R. L. Penn, *Science*, 2000, **289**, 751–754.

23 J. Polleux, N. Pinna, M. Antonietti and M. Niederberger, *Adv. Mater.*, 2004, **16**, 436–439.

24 A. Halder and N. Ravishankar, *Adv. Mater.*, 2007, **19**, 1854–1858.

25 Z. Tang, N. A. Kotov and M. Giersig, *Science*, 2002, **297**, 237–240.

26 K. S. Cho, D. V. Talapin, W. Gaschler and C. B. Murray, *J. Am. Chem. Soc.*, 2005, **127**, 7140–7147.

27 G. Zhu, S. Zhang, Z. Xu, J. Ma and X. Shen, *J. Am. Chem. Soc.*, 2011, **133**, 15605–15612.

28 Q. S. Liu, Z. Yan, N. L. Henderson, J. C. Bauer, D. W. Goodman, J. D. Batteas and R. E. Schaak, *J. Am. Chem. Soc.*, 2009, **131**, 5720–5721.

29 X. Chen, S. Shen, L. Guo and S. S. Mao, *Chem. Rev.*, 2010, **110**, 6503–6570.

30 A. Kudo and Y. Miseki, *Chem. Soc. Rev.*, 2009, **38**, 253–278.

31 Y. Wang, X. Wang and M. Antonietti, *Angew. Chem., Int. Ed.*, 2012, **51**, 68–89.

32 K. Maeda, X. Wang, Y. Nishihara, D. Lu, M. Antonietti and K. Domen, *J. Phys. Chem. C*, 2009, **113**, 4940–4947.

33 A. Kumar, S. Mandal, R. Pasricha, A. B. Mandale and M. Sastry, *Langmuir*, 2003, **19**, 6277–6282.

34 A. Badia, W. Gao, S. Singh, L. Demers, L. Cuccia and L. Reven, *Langmuir*, 1996, **12**, 1262–1269.

35 A. R. Tao, S. Habas and P. D. Yang, *Small*, 2008, **4**, 310–325.

36 X. G. Peng, J. Wickham and A. P. Alivisatos, *J. Am. Chem. Soc.*, 1998, **120**, 5343–5344.

37 C. Pacholski, A. Kornowski and H. Weller, *Angew. Chem., Int. Ed.*, 2002, **41**, 1188–1191.

38 F. Dumestre, B. Chaudret, C. Amiens, M. C. Fromen, M. J. Casanove, P. Renaud and P. Zurcher, *Angew. Chem., Int. Ed.*, 2002, **41**, 4286–4289.

39 T. Kwon, M. Min, H. Lee and B. J. Kim, *J. Mater. Chem.*, 2011, **21**, 11956–11960.

40 L. C. Ciacchi, W. Pompe and A. De Vita, *J. Am. Chem. Soc.*, 2001, **123**, 7371–7380.

41 L. C. Ciacchi, W. Pompe and A. De Vita, *J. Phys. Chem. B*, 2003, **107**, 1755–1764.

42 Z. M. Peng, H. J. You and H. Yang, *ACS Nano*, 2010, **4**, 1501–1510.

43 E. V. Shevchenko, D. V. Talapin, H. Schnablegger, A. Kornowski, O. Festin, P. Svedlindh, M. Haase and H. Weller, *J. Am. Chem. Soc.*, 2003, **125**, 9090–9101.

44 P. A. Rupar, L. Chabanne, M. A. Winnik and I. Manners, *Science*, 2012, **337**, 559–562.

45 M. L. S. Albuquerque, I. Guedes, R. Alcantara and S. G. C. Moreira, *Vib. Spectrosc.*, 2003, **33**, 127–131.

46 J. M. Serratos, W. D. Johns and A. Shimoyama, *Clays Clay Miner.*, 1970, **18**, 107–113.

47 A. H. M. Sondag and M. C. Raas, *J. Chem. Phys.*, 1989, **91**, 4926–4931.

48 T. Mishra, R. K. Sahu, S. H. Lim, L. G. Salamanca-Riba and S. Bhattacharjee, *Mater. Chem. Phys.*, 2010, **123**, 540–545.

49 M. V. Smoluchowski, *Z. Phys. Chem.*, 1917, **92**, 129–168.

50 J. Zhang, Y. Wang, J. Zheng, F. Huang, D. Chen, Y. Lan, G. Ren, Z. Lin and C. Wang, *J. Phys. Chem. B*, 2007, **111**, 1449–1454.

51 E. M. Hendriks and M. H. Ernst, *J. Colloid Interface Sci.*, 1984, **97**, 176–194.

52 J. Zhang, F. Huang and Z. Lin, *Nanoscale*, 2010, **2**, 18–34.

53 J. A. Edgar, A. M. McDonagh and M. B. Cortie, *ACS Nano*, 2012, **6**, 1116–1125.

54 D. R. Lide, *CRC handbook of chemistry and physics*, CRC Press, 2008.

55 X. X. Xu, G. Liu, C. Randorn and J. T. S. Irvine, *Int. J. Hydrogen Energy*, 2011, **36**, 13501–13507.

56 X. X. Xu, A. K. Azad and J. T. S. Irvine, *Catal. Today*, 2013, **199**, 22–26.